



Front-illuminated surface plasmon resonance biosensor for the study of light-responsive proteins and their interactions

Giusy Finocchiaro ^a, Aditya Suresh Chaudhari ^b, Tomáš Špringer ^a, Kateřina Králová ^a, Karel Chadt ^a, Erika Hemmerová ^a, Jan Bukáčěk ^a, Phuong Ngoc Pham ^b, Aditi Chatterjee ^b, Bohdan Schneider ^b, Gustavo Fuertes ^{b,*}, Jiří Homola ^{a,**}

^a Institute of Photonics and Electronics of the Czech Academy of Sciences, Chaberská 1014/57, 182 00, Prague, Czech Republic

^b Institute of Biotechnology of the Czech Academy of Sciences, Průmyslová 595, 252 50, Vestec, Czech Republic

ARTICLE INFO

Keywords:

Surface plasmon resonance
Photosensory proteins
Protein–protein interactions
Protein–DNA interactions
Non-canonical amino acids

ABSTRACT

Light-responsive proteins are involved in a wide range of essential physiological processes in bacteria, plants, and animals. Engineered light-responsive proteins have also emerged as prospective tools in biotechnology and biomedicine. These proteins are often characterized by short-lived lit states and the need for continuous illumination to reach photostationary states. Therefore, developing methods for studying light-responsive proteins and their interactions under illumination represents an important research goal. Here, we report on a novel front-illuminated surface plasmon resonance (fiSPR) biosensor for monitoring interactions involving light-responsive proteins. The fiSPR biosensor combines the optical platform based on the Kretschmann geometry with advanced transparent microfluidics and an additional light module, enabling *in situ* illumination of the liquid sample in contact with the SPR chip. We apply the fiSPR biosensor to study the blue light-responsive transcription factor EL222, which recovers to the dark state in a few seconds and plays an important role in the optogenetic control of gene expression. Specifically, we determine the rate and equilibrium constants for EL222 dimerization and DNA binding. The results support the hypothesis that EL222 dimerizes prior to binding DNA. In addition, we provide evidence of the interaction between an interleukin receptor modified with a photocaged tyrosine (IL-20R2-Y70NBY) and its cytokine ligand (IL-24) only upon UV illumination. Overall, this study demonstrates the versatility of the developed fiSPR biosensor for monitoring biomolecular interactions involving both natural and engineered light-responsive proteins, particularly those featuring short lit-state lifetimes.

1. Introduction

Light-responsive proteins are crucial for regulating essential physiological processes (Kottke et al., 2018), including adaptation to changing environmental conditions for bacteria (Padmanabhan et al., 2019), growth for plants (Pham et al., 2018), and vision and circadian rhythms for animals (Ozturk et al., 2011). Synthetic and engineered light-responsive proteins have also been developed as emerging tools for photocontrolling physiological processes, holding potential for applications in biotechnology and biomedicine (Charette et al., 2025; Seong and Lin, 2021; Zhu et al., 2025). These proteins typically undergo reversible conformational changes in response to light of specific wavelengths, enabling their interaction with other biomolecules, such as

proteins, genes, lipid membranes, or small ligands (Glantz et al., 2018; Kottke et al., 2018).

Numerous methods have been employed to investigate the structural properties of light-responsive proteins, including X-ray diffraction (XRD) and various optical spectroscopies (Hunt, 2024; Kukura et al., 2007; Poddar et al., 2022). Microplate readers combined with matrices of light-emitting diodes (LEDs) have been utilized for the high-throughput spectroscopic characterization of light-responsive proteins (Bugaj and Lim, 2019; Richter et al., 2015; Vogt et al., 2024). While these approaches provide valuable insights into molecular properties, they fail to deliver robust kinetic characterization of interactions involving light-responsive proteins. Other methods, such as nuclear magnetic resonance (NMR), size exclusion chromatography (SEC), and

* Corresponding author.

** Corresponding author.

E-mail addresses: gustavo.fuertes@ibt.cas.cz (G. Fuertes), homola@ufe.cz (J. Homola).

<https://doi.org/10.1016/j.bios.2025.117998>

Received 6 May 2025; Received in revised form 5 September 2025; Accepted 13 September 2025

Available online 16 September 2025

0956-5663/© 2025 The Authors. Published by Elsevier B.V. This is an open access article under the CC BY license (<http://creativecommons.org/licenses/by/4.0/>).

electrophoretic mobility shift assay (EMSA), have been used to investigate protein–protein or protein–nucleic acid interactions triggered by light (Chaudhari et al., 2025; Rivera-Cancel et al., 2012; Zoltowski et al., 2013). However, these methods are typically limited to measuring the equilibrium binding states and do not allow for the real-time monitoring of biomolecular interactions. An approach based on transient grating (TG) spectroscopy has recently been used to study both protein–protein and protein–nucleic acid binding processes triggered by light (Takakado et al., 2017, 2018; Terazima, 2022). Although TG spectroscopy enables the determination of the association rate constants, it does not provide the dissociation rate constants of the studied interactions. In recent years, various biosensors have been proposed to investigate interactions between biomolecules or to measure their concentrations (Abbasi, 2025; Gatterdam et al., 2017; Špringer et al., 2025). Biosensors based on biolayer interferometry (BLI) (Bates et al., 2025) have also been used as an alternative to conventional methods to study interactions involving light-responsive proteins (Carrasco-López et al., 2020; Gil et al., 2020). Among label-free optical biosensor techniques, surface plasmon resonance (SPR) biosensors represent one of the most advanced and versatile technologies for the kinetic analysis of biomolecular interactions, including protein–protein and protein–nucleic acid interactions (Ghiotto et al., 2010; Wang et al., 2015). Despite great advances made in the past two decades, SPR biosensors have not yet been applied to study light-responsive proteins, primarily due to the challenges associated with the need for simultaneous monitoring and *in situ* illumination of the interacting biomolecules.

Among light-responsive proteins, the blue light-responsive transcription factor EL222 from the bacterium *Erythrobacter litoralis* has recently attracted considerable attention as an optogenetic tool for controlling gene expression in both prokaryotic and eukaryotic cells (Cleere and Gardner, 2024; Jayaraman et al., 2016; Motta-Mena et al., 2014), with potential applications in biomedical research for cancer therapies, antimicrobials, and photodynamic therapies (Endres et al., 2018; Khorasanizadeh and Gardner, 2024; Pan et al., 2021; Sha et al.,

2024). EL222 presents two domains: (i) a photosensory light-oxygen-voltage (LOV) domain, and (ii) a DNA-binding helix–turn–helix (HTH) domain (Nash et al., 2011). The LOV domain embeds a flavin mononucleotide (FMN) chromophore, which absorbs blue light and triggers a reversible conformational change of EL222 from the dark to the lit state, with the latter being active for DNA binding (Nash et al., 2011). Although multiple studies have investigated EL222 structure and conformation (Andrikopoulos et al., 2021; Chaudhari et al., 2023, 2025; Iuliano et al., 2018; Liu et al., 2023; Nash et al., 2011), the kinetic aspects of interactions involving EL222 remain poorly explored. This is largely due to the short-lived lit state of EL222, estimated on the order of seconds (Nash et al., 2011; Zoltowski et al., 2013), which requires continuous sample illumination during measurements.

In this work, we report on a novel front-illuminated SPR (fiSPR) biosensor for real-time monitoring of interactions involving light-responsive proteins. The fiSPR biosensor combines the SPR sensing platform based on the Kretschmann geometry with advanced transparent microfluidics and a light module, which enables *in situ* illumination of the liquid sample in contact with the SPR chip. We apply the fiSPR biosensor to study the blue light-responsive transcription factor EL222. Specifically, we determine the rate and equilibrium constants for EL222 dimerization and DNA binding and investigate the mechanism of EL222–DNA interaction. In addition, we demonstrate the versatility of the fiSPR biosensor by monitoring the UV-triggered interaction between a light-responsive engineered interleukin receptor and its ligand.

2. fiSPR biosensor: principle of operation

The design and working principle of the fiSPR biosensor developed for light-assisted monitoring of biomolecular interactions are illustrated in Fig. 1. The optical sensing platform was implemented using attenuated total internal reflection in a prism coupler configured in the Kretschmann geometry and spectral modulation. In this configuration, a collimated beam of polychromatic light passes through the prism

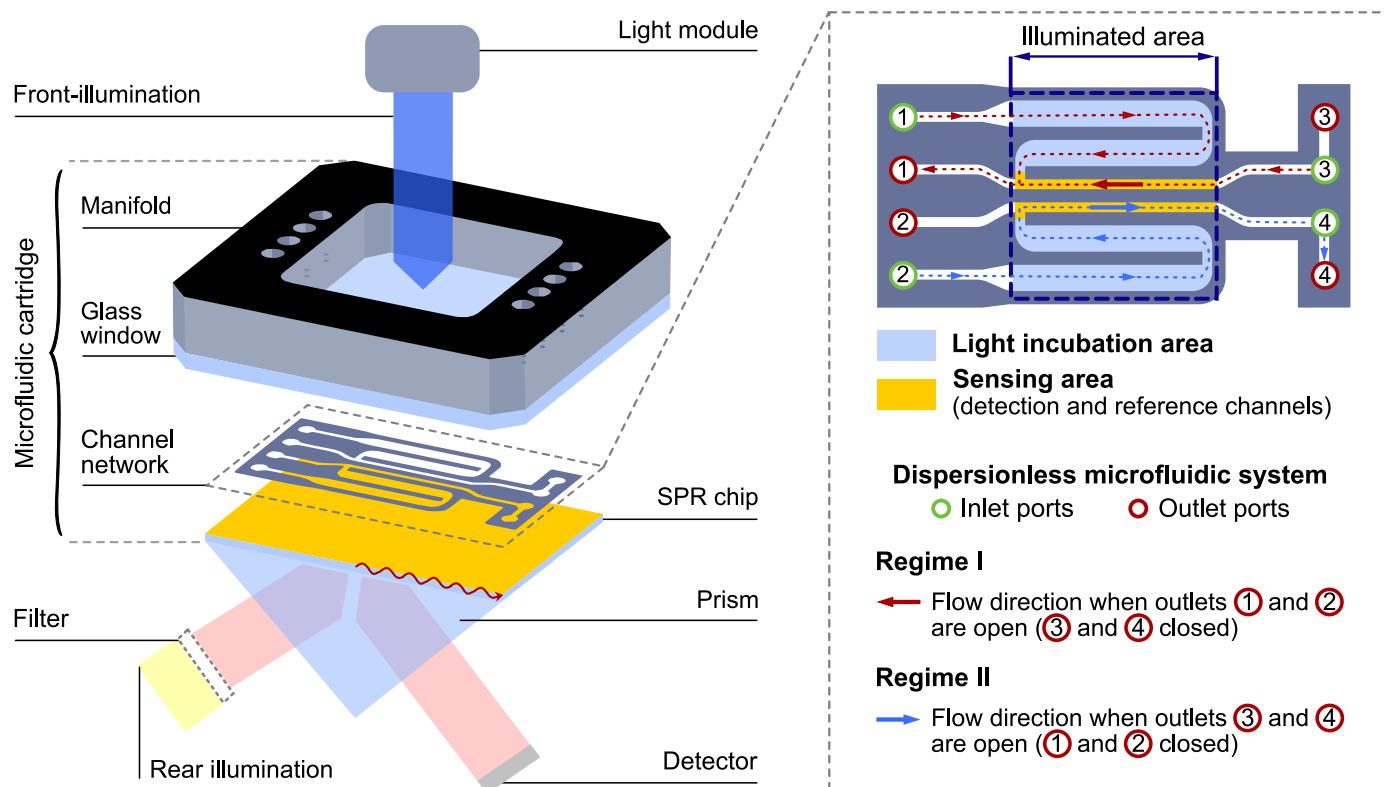


Fig. 1. Schematic of the fiSPR biosensor (left) and detail of the microfluidic system architecture (right).

coupler and illuminates the rear side of an SPR chip, generating surface plasmons at a specific wavelength. Their excitation results in a characteristic dip in the reflected light spectrum. The position of this dip is sensitive to local refractive index changes caused by biomolecular interactions near the sensor surface (Homola and Piliarik, 2006).

The SPR platform was integrated with a custom-designed microfluidic system and a light module to illuminate the SPR chip from the front side. This arrangement enabled the investigation of light-responsive proteins, which typically absorb light in a wavelength range from ~300 to 700 nm (see Table S1, Section S1 in Supplementary information, SI). This microfluidic system enabled precise delivery and controlled *in situ* illumination of target molecules. The microfluidic cartridge comprised three main elements: the SPR chip, a gasket defining a network of channels, and a manifold interfaced with the gasket through a transparent glass window. The channel network was organized into two distinct functional areas: the incubation area and the sensing area. In the incubation area, light-responsive proteins were exposed to illumination to trigger conformational changes essential for their biological activity. The proteins were then directed to the sensing area, where their interactions with the cognate receptors were monitored using the SPR technique. A reference-compensated sensing approach was implemented to ensure accurate and robust measurements, involving two functional regions in the sensing area. The first region was functionalized with the cognate receptor for detecting biomolecular interactions (detection channel). The second region was functionalized with a noncognate biomolecule to compensate for interfering effects, such as nonspecific binding or bulk refractive index changes (reference channel). The illumination of the light-responsive proteins was achieved using a narrow-band light source, which delivered light of a defined wavelength through the glass window of the microfluidic cartridge to the SPR chip.

3. Materials and methods

3.1. Implementation of fiSPR

The optical configuration of the fiSPR biosensor is illustrated in Fig. 1. The polychromatic light beam generated by a tungsten halogen bulb (HL-2000-HP-B, from Ocean Optics, Germany) was used in combination with a long-pass filter with a cutoff wavelength of 600 nm (FELH0600, from ThorLabs, Germany), to avoid unintended activation of the employed light-responsive protein. The light was collimated and directed onto the SPR chip at a fixed angle of 70° via a prism coupler to excite surface plasmons (Homola and Piliarik, 2006). The light reflected from the SPR chip was analyzed by a laboratory-made spectrometer containing a CMOS camera (acA1920-155um, from Basler, Germany). The dip in the spectrum of reflected light was tracked using dedicated software, with a 1 nm shift in its position corresponding to a protein surface density of 17 ng/cm² (Hemmerová et al., 2020). The SPR chip was obtained by coating a glass substrate (D 263® bio, 1.1 mm, from Schott, Germany) with 1.5 nm of titanium and 50 nm of gold by electron-beam evaporation in vacuum. The narrow-band light module used for illuminating light-responsive proteins consisted of an LED coupled with simple optics to produce a collimated light beam. The design allowed for easy replacement of the LED with LEDs emitting at different wavelengths. In this study, six LEDs were utilized (M365L3, M405LP1, M450LP1, M455L4, M490L4, M530L3, and M617L3, from ThorLabs, Germany). The light intensity was regulated using a dedicated LED driver (ThorLabs, Germany) and measured with an optical power meter (model 1916-C, from Newport, USA). The fiSPR sensing platform was enclosed in a balsa wood box with three BK7 glass windows (two on the sides for the polychromatic light source, and one on the front for the narrow-band light source) to provide thermal insulation. The temperature inside the box was maintained at 25 °C using a Peltier element.

The microfluidic system of the fiSPR biosensor was implemented as follows. The manifold of the microfluidic cartridge with four inlets and

four outlets was produced from polymethyl methacrylate (PMMA, from Plexiplast, Czech Republic). To avoid potential PMMA light-induced damage, the manifold was covered with a protective black foil (MACal 9800 PRO, from Refo, Czech Republic). The manifold was designed with a central glass window (D 263® bio, 1.1 mm), which was aligned with the sensing area and transparent to light in the 350–2650 nm range (Schott). The glass window was perforated at the inlet and outlet positions using a UV laser (Veles UVX, from Narran, Czech Republic) and attached to the manifold using two strips of double-sided adhesive gasket (Mylar foil with acrylic glue, from Fralock, USA), which were cut using a cutting plotter (Bengal 60, from Refo, Czech Republic). Another double-sided adhesive gasket featuring four channels (manufactured as above) was sandwiched between the SPR chip and the glass window. The design of the channel network followed the dispersionless microfluidics concept (Springer et al., 2010), which allowed for precise flow control and minimization of fluid intermixing. The used dispersionless microfluidics enabled two distinct operation regimes (Fig. 1): Regime I, in which the fluid flowed independently in all channels (with outlet ports 1 and 2 open, and 3 and 4 closed), and Regime II, in which the fluid from the incubation areas flowed into the sensing areas (with outlet ports 3 and 4 open, and 1 and 2 closed). Two peristaltic pumps (Ismatec® IPC, from Postnova, Germany) were used to pump the solutions through the microfluidic cartridge at adjustable flow rates.

3.2. Chemicals and buffers

The carboxy- and hydroxy-terminated alkanethiols (11-mercapto-hexa(ethyleneglycol)undecyloxy acetic acid (HS-C₁₁-(EG)₆-OCH₂-COOH) and 11-mercapto-tetra(ethyleneglycol)undecanol (HS-C₁₁-(EG)₄-OH), respectively) used to functionalize the SPR chip were purchased from Prochimia, Poland. Ethanamine hydrochloride (EA), 1-ethyl-3-(3-dimethylaminopropyl)-carbodiimide hydrochloride (EDC), and N-hydroxysuccinimide (NHS) were obtained from GE Healthcare, USA. Streptavidin, bovine serum albumin (BSA), and all other salts and buffers were purchased from Sigma-Aldrich, Germany, in molecular biology grade or higher purity. Strep-Tactin XT was purchased from IBA Lifesciences, Germany.

The buffers utilized in this study were prepared by dilution in deionized water (Q-water, 18 MΩ/cm resistivity, Direct-Q UV3, Millipore, USA) with the following compositions: 10 mM sodium acetate (SA₁₀), pH 5; phosphate buffer saline (PBS), pH 7.4, containing 1.4 mM KH₂PO₄, 8 mM Na₂HPO₄, 2.7 mM KCl, and 137 mM NaCl; high ionic strength PBS (PBS_{NaCl}), pH 7.4, containing 1.4 mM KH₂PO₄, 8 mM Na₂HPO₄, 2.7 mM KCl, and 750 mM NaCl; 50 mM tris(hydroxymethyl)aminomethane (Tris), pH 8, with the addition of 100 mM NaCl, and 1 mM phenylmethylsulfonyl fluoride (PMSF); and 50 mM 2-(N-morpholino)ethanesulfonic acid (MES), pH 6.8. MES_{BSA} was used as a running buffer for the fiSPR experiments with the following composition: 50 mM MES, 150 mM NaCl, 250 µg/ml BSA, and pH adjusted to 7.4 by adding NaOH. MES_{NaCl}, composed of 50 mM MES and 100 mM NaCl, pH 6.8, was used for EL222 storage, purification, microscale thermophoresis, Fourier-transformed IR spectroscopy, and UV-visible absorption spectroscopy. Tris_{BSA}, constituted of 50 mM Tris, 100 mM NaCl, and 250 µg/ml BSA, pH 8, was used for the storage and purification of the interleukins, and as a running buffer for the fiSPR experiments involving the interleukins.

The DNA sequences utilized for the fiSPR experiments were acquired from Sigma-Aldrich, Germany, and purified by desalting, except for the biotinylated sequences that were further purified by high-performance liquid chromatography (HPLC). All the proteins used in this study were recombinantly expressed in our laboratory. The gene encoding EL222 (kindly provided by Dr. Kevin Gardner) was expressed in *Escherichia coli* BL21 (DE3) as a fusion protein with a C-terminal intein-chitin binding domain-his tag (kindly provided by Dr. Edward Lemke). The terrific broth (TB) medium, carbenicillin, spectinomycin, isopropyl β-D-1-thiogalactopyranoside (IPTG), and dithiothreitol (DTT) were

purchased from Formedium, England. For genetic code expansion, we utilized the pDule2-CNF plasmid (Miyake-Stoner et al., 2009), which was provided by Dr. Ryan Mehl (Addgene plasmid #85495; <http://n2t.net/addgene:85495>; RRID:Addgene_85495). The full sequences of the utilized DNA and proteins, along with the protocols for the protein expression, purification, and modification, are provided in Section S2 in SI.

3.3. SPR chip functionalization and assays

The gold surface of the SPR chip was functionalized with a self-assembled monolayer (SAM) of alkanethiols by overnight immersion in an ethanolic solution containing a 3:7 M ratio of carboxy- and hydroxy-terminated alkanethiols at a total concentration of 200 μM , as described in (Hemmerová et al., 2020). Then, the chip was mounted in the SPR sensing platform and interfaced with the microfluidic cartridge. The carboxy-terminated alkanethiols were activated *in situ* with an aqueous solution of 25 mM NHS and 95.3 mM EDC for 10 min at 5 $\mu\text{l}/\text{min}$, followed by the injection of streptavidin in the sensing areas and BSA in the incubation areas for 15 min at 20 $\mu\text{l}/\text{min}$, which were dissolved in SA₁₀ to the final concentrations of 50 $\mu\text{g}/\text{ml}$ and 100 $\mu\text{g}/\text{ml}$, respectively. Streptavidin was employed for the oriented immobilization of biotinylated receptors, while BSA was used to prevent undesired nonspecific adsorption of EL222 in the incubation areas. PBS_{NaCl} was

subsequently flowed into all channels for 5 min at 20 $\mu\text{l}/\text{min}$ to remove the unbound proteins, followed by the injection of 0.5 M EA for 5 min at 20 $\mu\text{l}/\text{min}$ to block the unreacted carboxylic groups.

Two assays (Assays 1 and 2) were combined with the fiSPR biosensor to study the EL222–DNA system (Fig. 2). Assay 1 was designed to investigate EL222 binding to DNA. In Assay 1, the surfaces of the detection and reference channels were functionalized with biotinylated double-stranded and single-stranded DNA (b-dsDNA and b-ssDNA), respectively, followed by the injection of EL222 into both channels. Assay 1 was performed using the following protocol. First, a solution of 10 nM of the consensus b-ssDNA was prepared in PBS and injected into the detection and reference channels at 20 $\mu\text{l}/\text{min}$ until a surface density of $\sim 2 \cdot 10^{11}$ b-ssDNA/cm² was reached. Then, a solution of 40 nM of the complementary consensus ssDNA was prepared in MES_{BSA} and injected into the detection channel at 20 $\mu\text{l}/\text{min}$ to reach saturation ($\sim 1.7 \cdot 10^{11}$ ssDNA/cm²), forming b-dsDNA on the surface of the detection channel. The same immobilization conditions were applied to a scrambled DNA, obtained by shuffling the consensus DNA sequence (see Table S2 in SI). EL222 was subsequently injected into both detection and reference channels at varying conditions. To perform all the control and optimization experiments, EL222 was diluted in MES_{BSA} at a concentration of 1.5 μM and flowed over the functionalized sensor surfaces of both detection and reference channels for 10 min at 1.4 $\mu\text{l}/\text{min}$ (unless otherwise specified). To assess the optimal light exposure time of EL222,

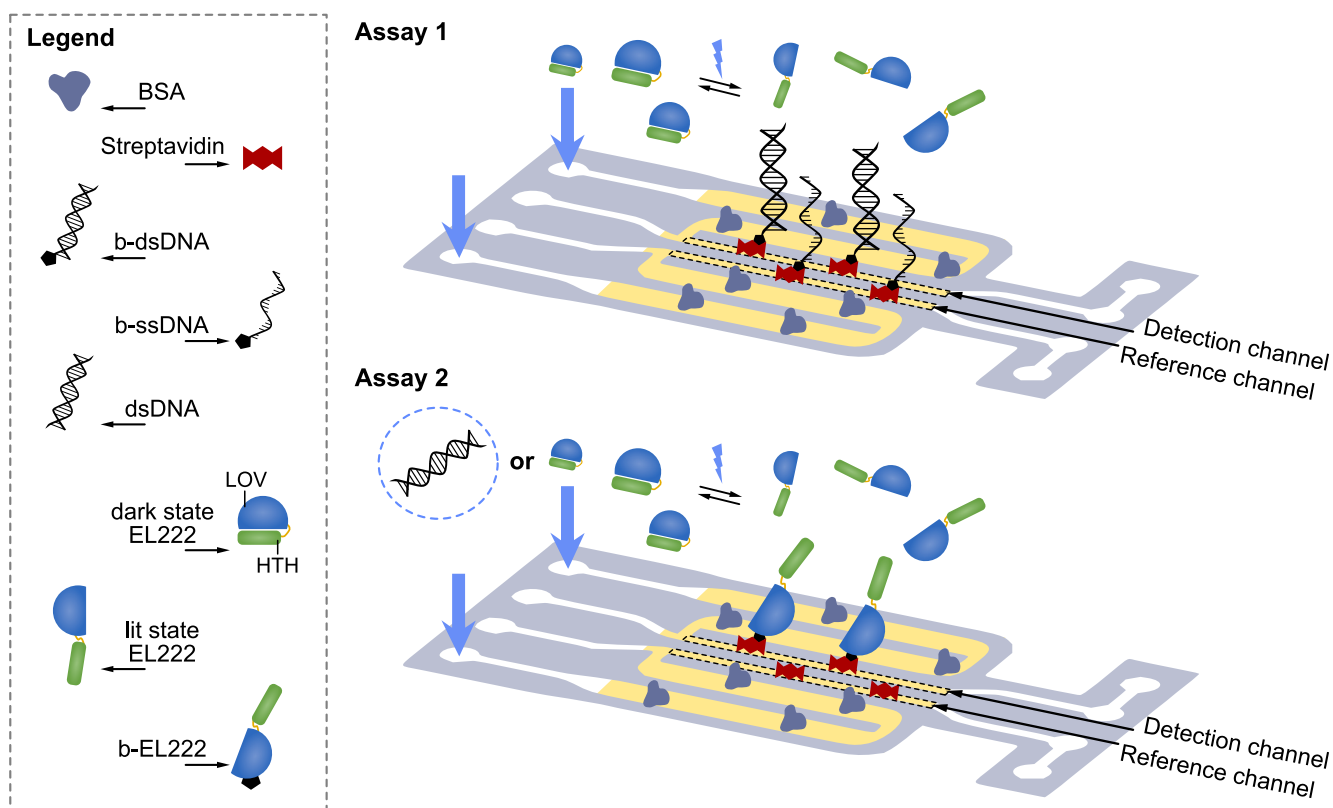


Fig. 2. Schematic of Assay 1 and Assay 2 (not drawn to scale). The illuminated area on the sensor surface is colored yellow. In Assay 1, EL222 was injected into both detection and reference channels. In Assay 2, either dsDNA or EL222 was injected into both channels. (For interpretation of the references to color in this figure legend, the reader is referred to the Web version of this article.)

1.5 μM EL222 in MES_{BSA} was flowed over the sensor surface for 10 min at flow rates of 1, 1.4, 2, 4, 9, and 20 $\mu\text{l}/\text{min}$. The light exposure time of EL222 was calculated by dividing the volume of the incubation area ($\sim 6 \mu\text{l}$) by the employed flow rate. For the analysis of the interaction between EL222 and b-dsDNA, solutions of 1, 1.5, 2, 3, and 4 μM EL222 were dissolved in MES_{BSA} and injected for 10 min at 1.4 $\mu\text{l}/\text{min}$ onto the functionalized sensor surfaces of both detection and reference channels. The experiments in which EL222 was illuminated *ex situ* were carried out by flowing 4 μM EL222 in MES_{BSA} after *ex situ* illumination for 600 s. Assay 2 was designed to investigate the interaction of EL222 monomer with DNA or with another EL222 monomer. In Assay 2, the surface of the detection channel was functionalized with biotinylated EL222 (b-EL222), and that of the reference channel was functionalized with streptavidin alone. The consensus dsDNA (or EL222) was subsequently injected into the detection and reference channels. Assay 2 was performed using the following protocol. First, a solution of 50 nM b-EL222 was prepared in PBS and flowed over the streptavidin-coated surface of the detection channel at 20 $\mu\text{l}/\text{min}$ until a surface density of $\sim 5 \cdot 10^{11}$ b-EL222/ cm^2 was reached. To verify whether a complex between an EL222 lit state monomer and the consensus dsDNA was formed, solutions of 5, 10, and 25 μM of dsDNA were prepared as described in Section S2 in SI, followed by a 3 min injection at 20 $\mu\text{l}/\text{min}$ into both detection and reference channels. To assess the kinetics of EL222 dimerization, solutions of 0.5, 1, 1.5, 2.5, and 5 μM EL222 were dissolved in MES_{BSA} and injected for 3 min at 4 $\mu\text{l}/\text{min}$ into both detection and reference channels. Assays 1 and 2 were performed under continuous illumination at a wavelength of 450 nm and a light intensity of 3.3 mW/cm^2 (unless otherwise specified). The illumination was initiated before flowing the sample (either EL222 in Assays 1 and 2, or DNA in Assay 2) over the functionalized sensor surface and maintained during both the association and dissociation phases. All presented sensor responses were reference-compensated by subtracting the sensor response of the reference channel from that of the detection channel. The error bars represent the standard deviation calculated from at least two independent fISPR experiments (for methodological details, see Section S3 in SI).

We also used the fISPR biosensor approach to monitor the interaction between an engineered mutant of an interleukin receptor (IL-20R2) and its ligand, the human interleukin 24 (IL-24). IL-20R2 was modified by replacing the tyrosine residue (Y) at position 70 with the light-responsive non-canonical amino acid *ortho*-nitrobenzyl-tyrosine (NBY), yielding IL-20R2-Y70NBY, as reported in Section S2 in SI. The obtained mutant was previously demonstrated to interact with IL-24 only upon UV illumination (Pham et al., 2023). To perform the fISPR experiment, we activated the carboxy-terminated alkanethiols as indicated above, followed by the injection into the sensing areas (for 15 min at 20 $\mu\text{l}/\text{min}$) of a solution of 50 $\mu\text{g}/\text{ml}$ of Strep-Tactin XT prepared in SA₁₀. IL-20R2-Y70NBY was subsequently immobilized on the sensor surface via the interaction between Twin-strep-tag, attached to the C-terminus of the engineered mutant (see Section S2 in SI), and Strep-Tactin XT (Schmidt et al., 2021). A solution of 100 nM of IL-20R2-Y70NBY was prepared in PBS and flowed over the surface of the detection channel until a surface density of $\sim 3 \cdot 10^{11}$ molecules/ cm^2 was reached. Finally, IL-24 was diluted in Tris_{BSA} to a concentration of 100 nM and injected into both the detection and reference channels for 10 min at 1.4 $\mu\text{l}/\text{min}$. IL-24 injection was performed in the absence of illumination and under *in situ* illumination with a wavelength of 365 nm, a light intensity of 8

mW/cm^2 , and a light exposure time of 260 s.

3.4. UV-visible absorption spectroscopy

The UV-visible absorption spectra (UV-vis spectra) of EL222 were recorded at room temperature using a nanophotometer (N60, from Implen, Germany), with 1 mm optical path length, and over a wavelength range from 200 to 900 nm. A solution of 195 μM EL222 was prepared in MES_{NaCl} , and its UV-vis spectrum was recorded without illumination, immediately after illumination, and after selected times from illumination (i.e., 10, 20, 40, 60, 90, and 120 s). The external light was generated by an LED module emitting at 450 nm with a light intensity of 3.3 mW/cm^2 .

4. Results and discussion

4.1. Effect of illumination on EL222–DNA system

The effect of illumination on the interaction between EL222 and DNA was investigated using Assay 1 (Fig. 2), in which EL222 was flowed over a DNA-modified sensor surface. Initially, we used Assay 1 to perform control experiments without illumination, with illumination (see Figs. S2a–b for the raw data), and with illumination of a scrambled DNA sequence immobilized on the sensor surface (Fig. 3a). EL222 was observed to bind to the consensus DNA only upon illumination, while its binding to the scrambled DNA or in the absence of light was negligible. These results indicate that EL222 did not form a stable complex with DNA in its dark state (Nash et al., 2011; Takakado et al., 2018), and that the *in situ* illumination triggered the specific binding of EL222 lit state to the consensus DNA sequence (Rivera-Cancel et al., 2012).

Subsequently, we performed experiments in which we immobilized the consensus DNA sequence on the sensor surface and then flowed EL222 along the sensor surface under various illumination conditions. In Fig. 3b, the results of the experiment, in which EL222 was illuminated with varying wavelengths (light exposure time: 260 s; light intensity: 1.5 mW/cm^2), are shown. The observed sensor response exhibited a clear dependence on the illumination wavelength, with the strongest EL222–DNA binding at 450 nm, and significantly weaker interaction at other wavelengths (365, 405, 490, 530, and 617 nm). Fig. 3c illustrates the observed wavelength dependence of the sensor response overlaid with the UV-vis spectrum of EL222 in its dark state. The spectral features of EL222, associated with the FMN chromophore, include a primary absorption band centered at 450 nm and a secondary band around 370 nm (Losi and Gartner, 2017). The minimal DNA binding observed upon illumination at 365 nm may be explained by the instability of EL222 lit state formed at this wavelength. In fact, the transition to EL222 lit state stems from the formation of a covalent adduct between the FMN and a close cysteine residue (Cys), which has been reported to break upon illumination at ~ 370 nm (Kennis et al., 2004). We also investigated the effect of varying light intensities at a fixed wavelength of 450 nm (light exposure time: 260 s). We observed that the sensor response to EL222–DNA binding increased with the light intensity until a maximum sensor response was reached at the values of 2.9 and 3.3 mW/cm^2 (Fig. 3d). Fig. S3 in SI (Section S4) reports the fraction of EL222 per DNA as a function of the light intensity and exposure time, which reached equilibrium after around 3 mW/cm^2 . Therefore, we selected a light

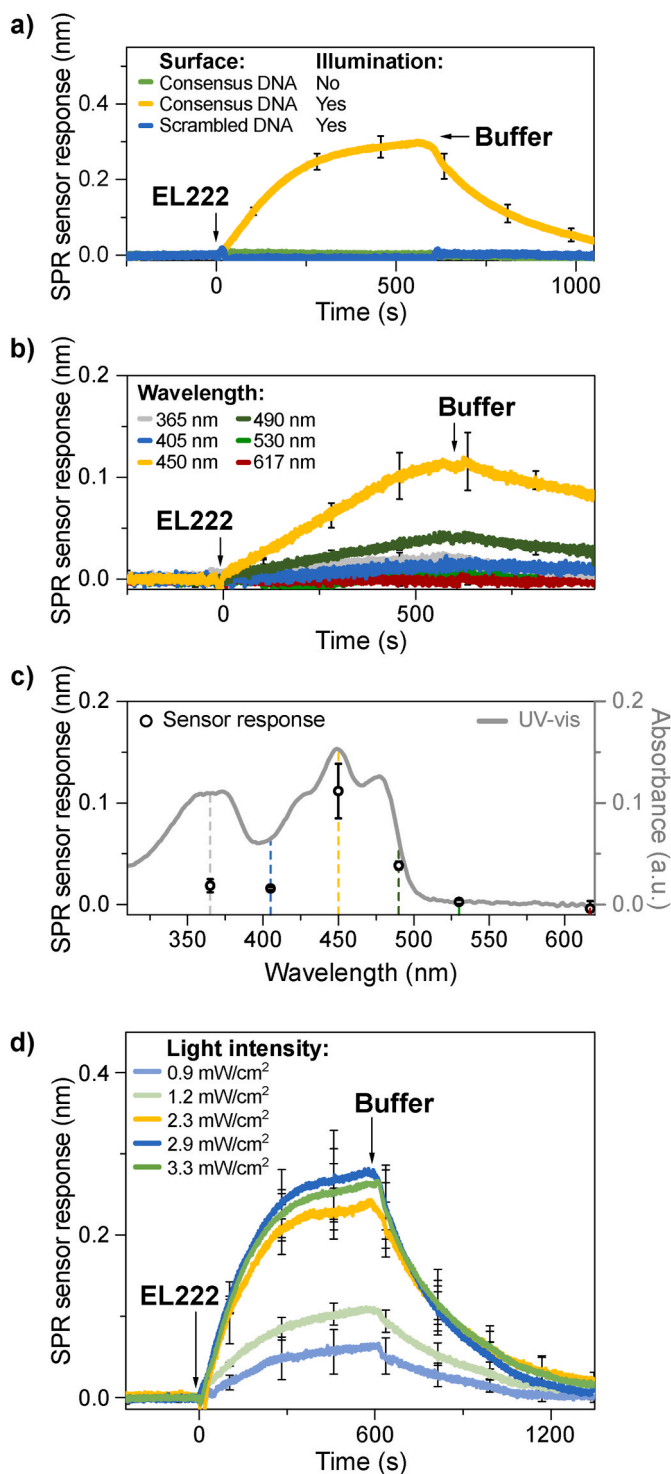


Fig. 3. Effect of illumination on EL222–DNA interaction. a) Reference-compensated sensor response to EL222 binding to the consensus DNA (without and with illumination), and to a scrambled DNA sequence (with illumination). b) Reference-compensated sensor response to EL222 binding to DNA under illumination at six different wavelengths, measured with the fiSPR biosensor. c) EL222–DNA sensor response as a function of the illumination wavelength, overlaid with the UV–vis spectrum of EL222 dark state (absorbance expressed in absorbance unit, a.u.). d) Reference-compensated sensor response to EL222 binding to DNA under illumination at five different light intensities, measured with the fiSPR biosensor.

intensity of 3.3 mW/cm^2 (with a wavelength of 450 nm) for all the subsequent fiSPR experiments with EL222 to minimize the influence of light intensity fluctuations. The selected value of light intensity was similar to those used for *in vivo* optogenetic studies, which typically span from ~ 0.1 to 10 mW/cm^2 (Cleere and Gardner, 2024; Hoffman et al., 2025; Motta-Mena et al., 2014).

4.2. Mechanism of interaction between EL222 and DNA

We used the fiSPR biosensor to investigate the mechanism of interaction between EL222 and DNA. To assess whether an EL222 lit state monomer could bind to DNA, we employed Assay 2 (Fig. 2), in which the DNA was flowed over an EL222-modified sensor surface. The results in Fig. 4a suggest that the DNA did not significantly bind to EL222 lit state monomers on the sensor surface.

To further investigate whether EL222 dimerization occurred before DNA binding, we used Assay 1 (Fig. 2), where EL222 was illuminated in the incubation area for varying durations before flowing over a DNA-modified sensor surface. As shown in Fig. 4b and Fig. S3 in SI, the binding of EL222 to DNA increased with the light exposure time until a maximum sensor response was reached for at least 260 s of illumination. Therefore, the subsequent experiments to study the kinetics of EL222–DNA interaction were performed by illuminating the sample for 260 s. To interpret the results in Fig. 4b, we recorded the UV–vis spectra of EL222 for selected light exposure times. The UV–vis spectrum of EL222 lit state is characterized by a decrease in the absorption band at 450 nm and the appearance of a new band around 390 nm , corresponding to the formation of the FMN–Cys covalent adduct (Losi and Gartner, 2017; Nash et al., 2011). The UV–vis spectra of EL222 in Fig. 4c obtained after varying light exposure times (from 15 to 360 s) exhibited the same absorbance values at 450 and 390 nm , suggesting a comparable population of EL222 lit states formed across all tested light exposure times. Therefore, the trend observed in Fig. 4b was not attributed to a growing number of EL222 lit state monomers captured by DNA, but to an increasing fraction of EL222 dimers forming at longer illumination times and binding to DNA. In addition, from the results in Fig. 4d, the dark recovery time of the band at 450 nm was determined to be below 40 s for all the explored illumination times of EL222 (from 15 to 360 s). These findings suggest the necessity of *in situ* illumination to prevent the transition from the active lit state (DNA binding) to the inactive dark state (no DNA binding) of EL222. To further stress this point, we measured the binding of EL222 to DNA at different times after *ex situ* illumination of EL222. The results in Fig. 4e show that the SPR sensor response due to the EL222 binding to DNA became smaller when the delay between the illumination and the measurement was prolonged. Particularly, a 3-min time after the illumination caused a significant decrease in EL222 binding to DNA, while a 30-min time resulted in a negligible interaction.

4.3. Kinetic analysis of EL222 dimerization

We used the fiSPR biosensor to determine the rate and equilibrium constants of EL222 dimerization. In these experiments, EL222 was immobilized on the sensor surface, and solutions containing different concentrations of EL222 were flowed over the surface (Assay 2, Fig. 2). The reference-compensated sensor response to EL222 forming dimers on the sensor surface is shown in Fig. 5. The reproducibility of the data was calculated to be about 84 % (for details, see Section S3 in SI). Initially, we fitted the obtained sensor response using a 1:1 Langmuir model, where an EL222 monomer in solution binds to an EL222 monomer immobilized on the sensor surface. However, this approach resulted in a rather poor fit (see Fig. S8 in SI). We then hypothesized that EL222 could change its conformation upon dimerization, as previously reported in other studies (Chaudhari et al., 2025; Zoltowski et al., 2013). To pursue this hypothesis, we conducted experiments using time-resolved IR (TRIR) spectroscopy and two EL222 mutants, including the isolated LOV

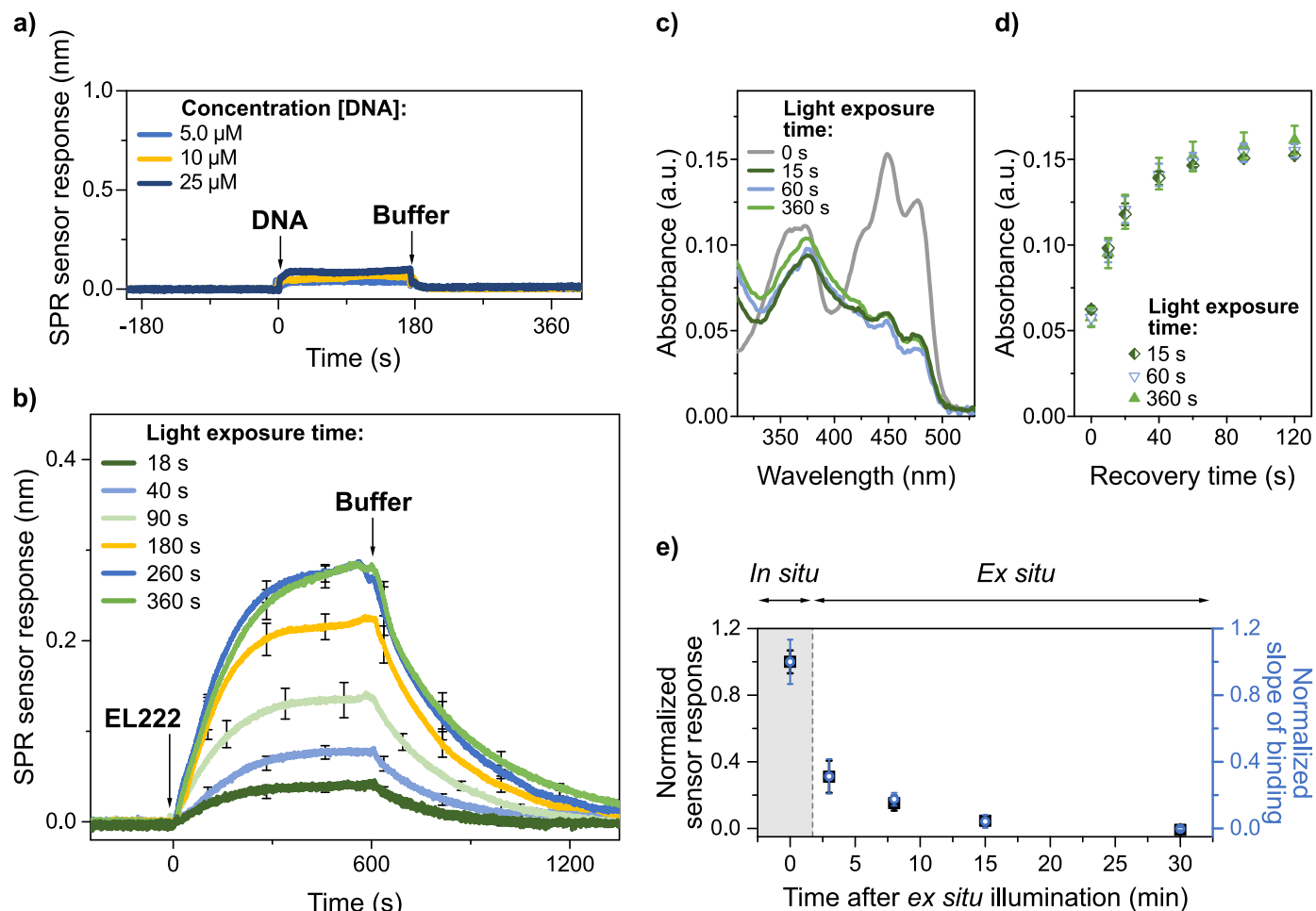


Fig. 4. Investigation of EL222–DNA interaction mechanism. a) Reference-compensated sensor response to the binding of DNA to EL222 lit state monomers immobilized on the sensor surface (under continuous illumination). b) Reference-compensated sensor response to EL222 binding to DNA under illumination for six different light exposure times, measured with the fiSPR biosensor. c) UV–vis spectra of EL222 illuminated for four different exposure times. d) Recovery time of the 450 nm absorption band in the dark after illumination of EL222 for three different exposure times. e) Normalized sensor response to EL222 binding to DNA as a function of the time after *ex situ* illumination, overlaid with the normalized binding slope.

domain (see Section S5 in SI). We observed that the dimerization of two isolated LOV domains could be fitted with a one-component exponential function, while EL222 dimerization seemed to follow a more complex interaction scheme, requiring a two-component exponential fit (see Fig. S4 in SI). The 1:1 interaction scheme of two isolated LOV domains was confirmed using the fiSPR biosensor (see Fig. S5 in SI). The overall results suggest the existence of two dimeric conformational states of EL222, possibly formed by the sequential dimerization of the individual EL222 domains (LOV and HTH) (Zoltowski et al., 2013). Consequently, we fitted the sensor response using a two-state binding model, in which the initially formed EL222 dimer (D1) relaxed into a more stable dimeric structure (D2). To account for EL222 dimer formation in solution, we fitted the sensor response using the equilibrium monomer bulk concentrations $[M]_{eq}$ instead of the initial monomer concentrations $[M]_0$. $[M]_{eq}$ was calculated by iterating the fitting cycles, as reported in Section S6 in SI (particularly, Fig. S6 illustrates $[M]_0$ and $[M]_{eq}$ as a function of the fitting cycle). Table 1 reports the rate and equilibrium

constants for the formation of D1 and subsequent relaxation into D2, which were determined by fitting the results using a two-state binding model with $[M]_{eq}$ as the equilibrium concentration (Fig. 5). To validate the results obtained with the fiSPR biosensor, we compared the association rate constant (k_a) of D1 formation ($\sim 2 \cdot 10^3 \text{ M}^{-1}\text{s}^{-1}$) with the k_a determined by TG spectroscopy ($\sim 9 \cdot 10^3 \text{ M}^{-1}\text{s}^{-1}$) (Takakado et al., 2017, 2018) and found them to be in good agreement.

4.4. Kinetic analysis of interaction between EL222 dimer and DNA

We used the fiSPR biosensor to determine the rate and equilibrium constants of the interaction between EL222 dimer and DNA. In these experiments, the DNA was immobilized on the sensor surface, and EL222 flowed over the surface (Assay 1, Fig. 2). We measured the sensor response to different concentrations of EL222 dimer binding to DNA (Fig. 6). The reproducibility of the data was calculated to be about 82 % (for details, see Section S3 in SI). We fitted the results with a 1:1

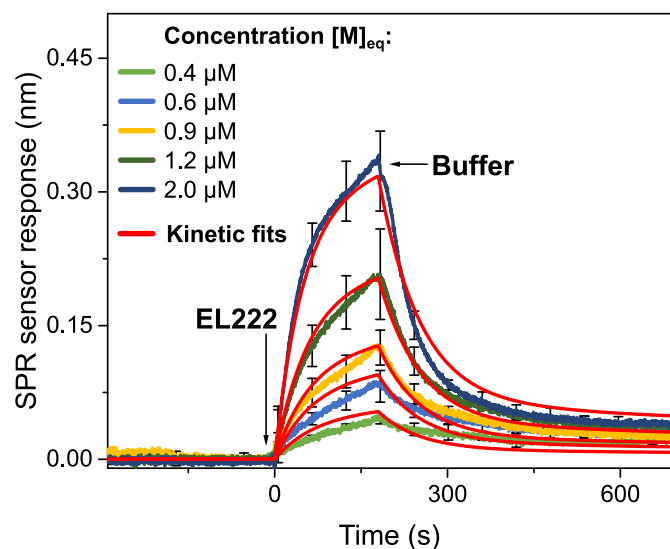


Fig. 5. Reference-compensated sensor response to different concentrations of EL222 monomers forming dimers on the sensor surface, measured with the fiSPR biosensor. The red curves represent the least-squares fit of the sensor response using a two-state binding model, with $[M]_{eq}$ as the equilibrium concentrations. (For interpretation of the references to color in this figure legend, the reader is referred to the Web version of this article.)

Langmuir model, where an EL222 dimer in solution binds to a DNA molecule immobilized on the surface. The total concentration of EL222 dimer in solution ($[D]_{eq}$) was determined as explained in Section S6 in SI. Particularly, Fig. S7 shows the equilibrium concentrations of different species present in solution ($[M]_{eq}$, $[D1]_{eq}$, $[D2]_{eq}$, and $[D]_{eq}$), normalized to $[M]_0$ and plotted as a function of $[M]_0$. Table 2 reports the determined rate and equilibrium constants of the interaction between EL222 dimer and DNA. The equilibrium dissociation constant ($K_D \sim 700$ nM) was found to be in close agreement with the half maximal effective concentration (EC_{50}) previously determined using EMSA and a similar DNA sequence (~ 400 nM) (Rivera-Cancel et al., 2012). To further validate the fiSPR results, we investigated the interaction between EL222 dimer and DNA with a commercially available BLI system (Bates et al., 2025). The k_a value obtained using the BLI approach was lower than that obtained using the fiSPR approach, which we attribute to the fact that, in the BLI platform, the illumination was limited only to the period prior to the binding experiment (Fig. 7, see the experimental details in Section S7 in SI). We also performed experiments using microscale thermophoresis to confirm the importance of *in situ* illumination of the sample (see Fig. S9 in SI). The overall findings of this study (Figs. 3–7) support the dimer pathway hypothesis, in which EL222 dimerizes prior to binding DNA, as depicted in Fig. S10, Section S8 in SI.

Table 1

Rate and equilibrium constants of EL222 dimerization. The values were averaged from 3 independent experiments. Abbreviations: k_a - association rate constant; k_d - dissociation rate constant; K_D - equilibrium dissociation constant; M_{eq} - lit state EL222 monomer at equilibrium; M - EL222 monomer immobilized on the sensor surface; D1 - transient EL222 dimer; D2 - stable conformation of EL222 dimer.

Interaction	k_a	k_d	K_D
$M_{eq} + M \rightleftharpoons D1$	$(1.68 \pm 0.44) \cdot 10^3 \text{ M}^{-1} \text{ s}^{-1}$	$(1.31 \pm 0.00) \cdot 10^{-2} \text{ s}^{-1}$	$(8.14 \pm 1.81) \mu\text{M}$
$D1 \rightleftharpoons D2$	$(1.13 \pm 0.00) \cdot 10^{-3} \text{ s}^{-1}$	$(7.17 \pm 0.67) \cdot 10^{-4} \text{ s}^{-1}$	0.63 ± 0.06

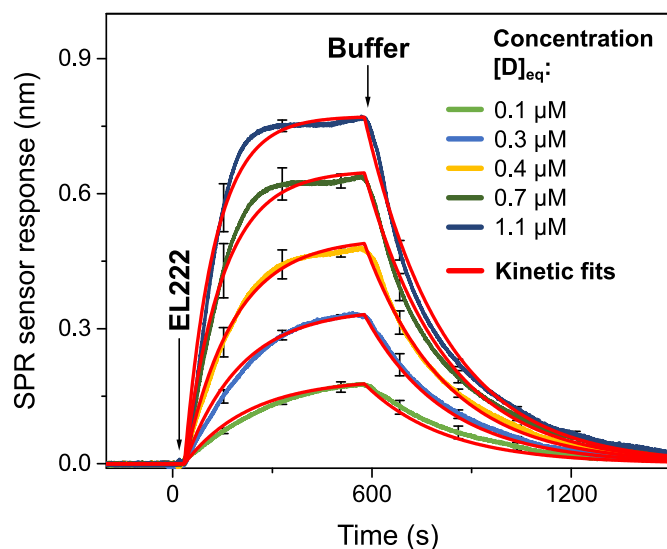


Fig. 6. Reference-compensated sensor response to different concentrations of EL222 dimers binding to DNA on the sensor surface, measured with the fiSPR biosensor. The red curves represent the least-squares fit of the sensor response using a 1:1 Langmuir model, with $[D]_{eq}$ as the equilibrium concentrations. (For interpretation of the references to color in this figure legend, the reader is referred to the Web version of this article.)

4.5. Study of interaction between IL-20R2-Y70NBY and IL-24

To demonstrate the versatility of the fiSPR biosensor, we monitored the interaction between an interleukin receptor modified with a photocaged tyrosine (IL-20R2-Y70NBY) and its cytokine ligand (IL-24). The molecular models of IL-20R2-Y70NBY and IL-24 and their interaction scheme are reported in Fig. S1 in SI. The results in Fig. 8 show that IL-24 was captured by IL-20R2-Y70NBY immobilized on the sensor surface only upon UV illumination, which triggers the activation of IL-20R2-Y70NBY. Conversely, the interaction was negligible in the absence of illumination, which is in excellent agreement with Ref. (Pham et al., 2023).

5. Conclusions

This work reports on a novel biosensing platform (fiSPR) for monitoring interactions involving light-responsive proteins. The fiSPR biosensor combines the optical platform based on the Kretschmann geometry with advanced transparent microfluidics and an additional light module on the front side. Such a combination enables *in situ* continuous illumination of the sample in contact with the SPR chip. We demonstrate the unique capability of the fiSPR biosensor to monitor interactions

Table 2

Rate and equilibrium constants of EL222–DNA interaction. The values were averaged from 4 independent experiments. Abbreviations: k_a - association rate constant; k_d - dissociation rate constant; K_D - equilibrium dissociation constant; D_{eq} - total EL222 dimer at equilibrium; DNA - DNA immobilized on the sensor surface; D–DNA - complex formed between EL222 dimer and DNA.

Interaction	k_a	k_d	K_D
$D_{eq} + DNA \rightleftharpoons D-DNA$	$(6.47 \pm 1.29) \cdot 10^3 \text{ M}^{-1}\text{s}^{-1}$	$(4.40 \pm 0.64) \cdot 10^{-3} \text{ s}^{-1}$	$(0.70 \pm 0.18) \mu\text{M}$

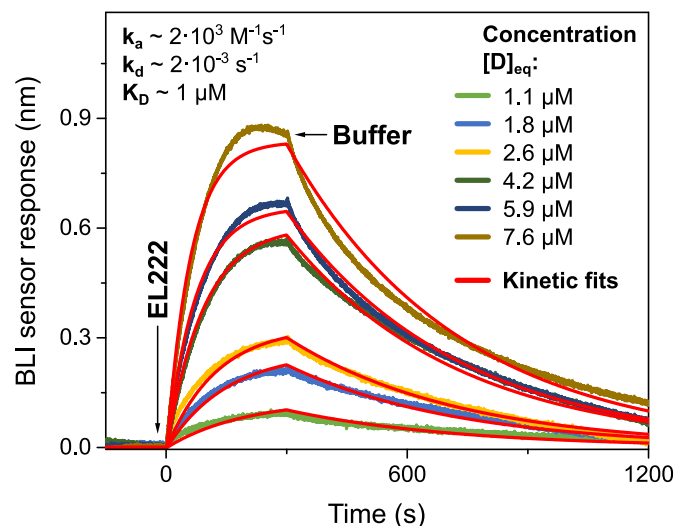


Fig. 7. Reference-compensated sensor response to different concentrations of EL222 dimers binding to DNA on the sensor surface, measured with a commercial BLI platform. The red curves represent the least-squares fit of the sensor response using a 1:1 Langmuir model, with $[D]_{eq}$ as the equilibrium concentrations. (For interpretation of the references to color in this figure legend, the reader is referred to the Web version of this article.)

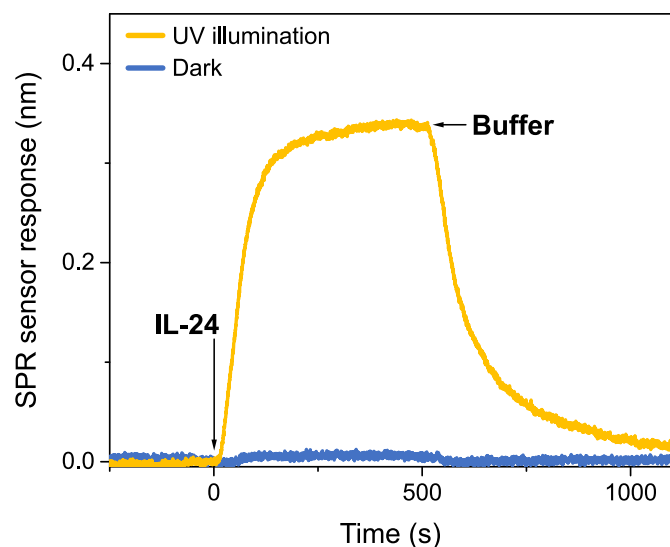


Fig. 8. Reference-compensated sensor response to IL-24 binding to IL-20R2-Y70NBY immobilized on the sensor surface, without and with UV illumination.

involving light-responsive proteins with short-lived lit states, such as EL222. For the first time, we provide a comprehensive kinetic analysis of EL222 dimerization and DNA binding. Our findings support the dimer pathway hypothesis, which suggests that EL222 dimerizes prior to interacting with DNA. Furthermore, we show that the fiSPR biosensing platform holds potential for studying synthetic light-responsive proteins, including engineered receptor–interleukin pairs and possibly

other optogenetic systems. As such, the fiSPR biosensor represents a versatile and powerful tool for advancing research in optogenetics and biomedicine.

CRediT authorship contribution statement

Giusey Finocchiaro: Writing – original draft, Methodology, Investigation, Conceptualization. **Aditya Suresh Chaudhari:** Writing – review & editing, Methodology. **Tomáš Špringer:** Writing – review & editing, Supervision, Conceptualization. **Kateřina Králová:** Writing – review & editing, Methodology, Investigation. **Karel Chadt:** Writing – review & editing, Methodology. **Erika Hemmerová:** Writing – review & editing, Methodology. **Jan Bukáček:** Writing – review & editing, Methodology. **Phuong Ngoc Pham:** Methodology, Investigation. **Aditi Chatterjee:** Methodology, Investigation. **Bohdan Schneider:** Writing – review & editing, Funding acquisition. **Gustavo Fuertes:** Writing – review & editing, Supervision, Funding acquisition, Conceptualization. **Jiří Homola:** Writing – review & editing, Supervision, Funding acquisition, Conceptualization.

Declaration of generative AI and AI-assisted technologies in the writing process

During the preparation of the first draft of the manuscript (i.e., the Introduction and Section 4.1 of Results and discussion), the first author used ChatGPT exclusively to improve language and grammar, in compliance with the AI policies of the journal. Subsequently, all authors have expanded and edited the text as necessary and take full responsibility for the content of the publication.

Declaration of competing interest

The authors declare that they have no known competing financial interests or personal relationships that could have appeared to influence the work reported in this paper.

Acknowledgements

This study was supported by the National Institute for Cancer Research (Programme EXCELES, ID Project No. LX22NPO5102) – Funded by the European Union – Next Generation EU, and by the Czech Science Foundation, contracts 20-23787X, 22-27329S, and 24-11819S. The Institute of Biotechnology of the Czech Academy of Sciences acknowledges the institutional grant RVO86652036. We acknowledge CF Biophysics, CF SMS of CIISB, Instruct-CZ Centre BIOCEV, supported by MEYS CR (LM2023042) and ERDF-Project “Innovation of Czech Infrastructure for Integrative Structural Biology” (No. CZ.02.01.01/00/23_015/0008175). The illustrations in this article were created with Inkscape.

Appendix A. Supplementary data

Supplementary data to this article can be found online at <https://doi.org/10.1016/j.bios.2025.117998>.

Data availability

The data are available at the link <https://doi.org/10.5281/zenodo.15847931>.

References

- Abbasi, E., 2025. Biological sensors and bio-inspired technologies: the role of insects in advanced detection systems and robotics. *Discov. Appl. Sci.* 7 (6), 503.
- Andrikopoulos, P.C., Chaudhari, A.S., Liu, Y., Konold, P.E., Kennis, J.T., Schneider, B., Fuentes, G., 2021. QM calculations predict the energetics and infrared spectra of transient glutamine isomers in LOV photoreceptors. *Phys. Chem. Chem. Phys.* 23 (25), 13934–13950.
- Bates, T.A., Gurmessa, S.K., Weinstein, J.B., Trank-Greene, M., Wrynla, X.H., Anastas, A., Anley, T.W., Hinchliff, A., Shinde, U., Burke, J.E., 2025. Biolayer interferometry for measuring the kinetics of protein–protein interactions and nanobody binding. *Nat. Protoc.* 20 (4), 861–883.
- Bugaj, L.J., Lim, W.A., 2019. High-throughput multicolor optogenetics in microwell plates. *Nat. Protoc.* 14 (7), 2205–2228.
- Carrasco-López, C., Zhao, E.M., Gil, A.A., Alam, N., Toettcher, J.E., Avalos, J.L., 2020. Development of light-responsive protein binding in the monobody non-immunoglobulin scaffold. *Nat. Commun.* 11 (1), 4045.
- Charette, M., Rosenblum, C., Shade, O., Deiters, A., 2025. Optogenetics with atomic precision—A comprehensive review of optical control of protein function through genetic code expansion. *Chem. Rev.*
- Chaudhari, A.S., Chatterjee, A., Domingos, C.A.O., Andrikopoulos, P.C., Liu, Y., Andersson, I., Schneider, B., Lorenz-Fonfria, V.A., Fuentes, G., 2023. Genetically encoded non-canonical amino acids reveal asynchronous dark reversion of chromophore, backbone, and side-chains in EL222. *Protein Sci.* 32 (4), e4590.
- Chaudhari, A.S., Favier, A., Tehrani, Z.A., Kovář, T., Andersson, I., Schneider, B., Dohnálek, J., Černý, J., Brutscher, B., Fuentes, G., 2025. Light-dependent flavin redox and adduct states control the conformation and DNA-Binding activity of the transcription factor EL222. *Nucleic Acids Res.* 53 (6), gkaf215.
- Cleere, M.M., Gardner, K.H., 2024. Optogenetic control of phosphate-responsive genes using single-component fusion proteins in *Saccharomyces cerevisiae*. *ACS Synth. Biol.* 13 (12), 4085–4098.
- Endres, S., Wingen, M., Torra, J., Ruiz-González, R., Polen, T., Bosio, G., Bitzenhofer, N. L., Hilgers, F., Gensch, T., Nonell, S., 2018. An optogenetic toolbox of LOV-Based photosensitizers for light-driven killing of bacteria. *Sci. Rep.* 8 (1), 15021.
- Gatterdam, V., Frutiger, A., Stengele, K.-P., Heindl, D., Lübbers, T., Vörös, J., Fattinger, C., 2017. Focal microscopy is a new method for the in situ analysis of molecular interactions in biological samples. *Nat. Nanotechnol.* 12 (11), 1089–1095.
- Ghiotto, M., Gauthier, L., Serriari, N., Pastor, S., Truneh, A., Nunes, J.A., Olive, D., 2010. PD-L1 and PD-L2 differ in their molecular mechanisms of interaction with PD-1. *Int. Immunol.* 22 (8), 651–660.
- Gil, A.A., Carrasco-López, C., Zhu, L., Zhao, E.M., Ravindran, P.T., Wilson, M.Z., Aaglia, A.G., Avalos, J.L., Toettcher, J.E., 2020. Optogenetic control of protein binding using light-switchable nanobodies. *Nat. Commun.* 11 (1), 4044.
- Glantz, S.T., Berlew, E.E., Jaber, Z., Schuster, B.S., Gardner, K.H., Chow, B.Y., 2018. Directly light-regulated binding of RGS-LOV photoreceptors to anionic membrane phospholipids. *Proc. Natl. Acad. Sci.* 115 (33), E7720–E7727.
- Hemmerová, E., Špringer, T., Křištofiková, Z., Homola, J., 2020. Study of biomolecular interactions of mitochondrial proteins related to alzheimer's disease: toward multi-interaction biomolecular processes. *Biomolecules* 10 (9).
- Hoffman, S.M., Espinel-Rios, S., Kwartler, S.K., Lalwani, M.A., Avalos, J.L., 2025. Balancing doses of EL222 and light improves optogenetic induction of protein production in *Komagataella phaffii*. *Biotechnol. Bioeng.*
- Homola, J., Piliarik, M., 2006. *Surface Plasmon Resonance (SPR) Sensors*. Springer.
- Hunt, N.T., 2024. Biomolecular infrared spectroscopy: making time for dynamics. *Chem. Sci.* 15 (2), 414–430.
- Iuliano, J.N., Gil, A.A., Laptanok, S.P., Hall, C.R., Tolentino Collado, J., Lukacs, A., Hag Ahmed, S.A., Abyad, J., Daryaei, T., Greetham, G.M., 2018. Variation in LOV photoreceptor activation dynamics probed by time-resolved infrared spectroscopy. *Biochemistry* 57 (5), 620–630.
- Jayaraman, P., Devarajan, K., Chua, T.K., Zhang, H., Gunawan, E., Poh, C.L., 2016. Blue light-mediated transcriptional activation and repression of gene expression in bacteria. *Nucleic Acids Res.* 44 (14), 6994–7005.
- Kennis, J.T., Van Stokkum, L.H., Crosson, S., Gauden, M., Moffat, K., van Grondelle, R., 2004. The LOV2 domain of phototropin: a reversible photochromic switch. *J. Am. Chem. Soc.* 126 (14), 4512–4513.
- Khorasanizadeh, S., Gardner, K.H., 2024. Mechanisms of PAS Domain Signalling, from Sensing Varied Small Molecules and Peptides to Approved Pharmaceuticals and Use in Optogenetics, 168457.
- Kottke, T., Xie, A., Larsen, D.S., Hoff, W.D., 2018. Photoreceptors take charge: emerging principles for light sensing. *Annu. Rev. Biophys.* 47 (1), 291–313.
- Kukura, P., McCamant, D.W., Mathies, R.A., 2007. Femtosecond stimulated raman spectroscopy. *Annu. Rev. Phys. Chem.* 58 (1), 461–488.
- Liu, Y., Chaudhari, A.S., Chatterjee, A., Andrikopoulos, P.C., Picchiotti, A., Rebarz, M., Kloz, M., Lorenz-Fonfria, V.A., Schneider, B., Fuentes, G., 2023. Sub-Millisecond photoinduced dynamics of free and EL222-Bound FMN by stimulated raman and visible absorption spectroscopies. *Biomolecules* 13 (1).
- Losi, A., Gartner, W., 2017. Solving blue light riddles: new lessons from flavin-binding LOV photoreceptors. *Photochem. Photobiol.* 93 (1), 141–158.
- Miyake-Stoner, S.J., Miller, A.M., Hammill, J.T., Peeler, J.C., Hess, K.R., Mehl, R.A., Brewer, S.H., 2009. Probing protein folding using site-specifically encoded unnatural amino acids as FRET donors with tryptophan. *Biochemistry* 48 (25), 5953–5962.
- Motta-Mena, L.B., Reade, A., Mallory, M.J., Glantz, S., Weiner, O.D., Lynch, K.W., Gardner, K.H., 2014. An optogenetic gene expression system with rapid activation and deactivation kinetics. *Nat. Chem. Biol.* 10 (3), 196–202.
- Nash, A.I., McNulty, R., Shillito, M.E., Swartz, T.E., Bogomolni, R.A., Luecke, H., Gardner, K.H., 2011. Structural basis of photosensitivity in a bacterial light-oxygen-voltage/helix-turn-helix (LOV-HTH) DNA-binding protein. *Proc. Natl. Acad. Sci. U. S. A.* 108 (23), 9449–9454.
- Ozturk, N., Selby, C.P., Annayev, Y., Zhong, D., Sancar, A., 2011. Reaction mechanism of drosophila cryptochrome. *Proc. Natl. Acad. Sci.* 108 (2), 516–521.
- Padmanabhan, S., Pérez-Castaño, R., Elías-Armanz, M., 2019. B12-based photoreceptors: from structure and function to applications in optogenetics and synthetic biology. *Curr. Opin. Struct. Biol.* 57, 47–55.
- Pan, H., Li, L., Pang, G., Han, C., Liu, B., Zhang, Y., Shen, Y., Sun, T., Liu, J., Chang, J., Wang, H., 2021. Engineered NIR light-responsive bacteria as anti-tumor agent for targeted and precise cancer therapy. *Chem. Eng. J.* 426.
- Pham, P.N., Zahradník, J., Kolářová, L., Schneider, B., Fuentes, G., 2023. Regulation of IL-24/IL-20R2 complex formation using photocaged tyrosines and UV light. *Front. Mol. Biosci.* 10, 1214235.
- Pham, V.N., Kathare, P.K., Huq, E., 2018. Phytochromes and phytochrome interacting factors. *Plant Physiol.* 176 (2), 1025–1038.
- Poddar, H., Heyes, D.J., Schirò, G., Weik, M., Leys, D., Scrutton, N.S., 2022. A guide to time-resolved structural analysis of light-activated proteins. *FEBS J.* 289 (3), 576–595.
- Richter, F., Scheib, U.S., Mehlhorn, J., Schubert, R., Wietek, J., Gernetzki, O., Hegemann, P., Mathes, T., Möglich, A., 2015. Upgrading a microplate reader for photobiology and all-optical experiments. *Photochem. Photobiol. Sci.* 14 (2), 270–279.
- Rivera-Cancel, G., Motta-Mena, L.B., Gardner, K.H., 2012. Identification of natural and artificial DNA substrates for light-activated LOV-HTH transcription factor EL222. *Biochemistry* 51 (50), 10024–10034.
- Schmidt, T.G.M., Eichinger, A., Schneider, M., Bonet, L., Carl, U., Karthaus, D., Theobald, I., Skerra, A., 2021. The role of changing loop conformations in streptavidin versions engineered for high-affinity binding of the *Strep-tag ii* peptide. *J. Mol. Biol.* 433 (9), 166893.
- Schott. **Material properties of D 263® bio.** <https://www.schott.com/en-gb/products/d-263-p1000318/technical-details?tab=830fa6759ac84d07a3d53bfe4535a90>.
- Seong, J., Lin, M.Z., 2021. Optobiochemistry: genetically encoded control of protein activity by light. *Annu. Rev. Biochem.* 90 (1), 475–501.
- Sha, N., Xu, S., Wan, B., Zhao, K.-H., 2024. Light-oxygen-voltage (LOV) domain-derived photosensitizers with the highest quantum yield for superoxide anion or singlet oxygen. *J. Photochem. Photobiol. Chem.* 452, 115591.
- Špringer, T., Bocková, M., Slabý, J., Sohrabi, F., Čapková, M., Homola, J., 2025. Surface plasmon resonance biosensors and their medical applications. *Biosens. Bioelectron.* 117308.
- Špringer, T., Piliarik, M., Homola, J., 2010. Surface plasmon resonance sensor with dispersionless microfluidics for direct detection of nucleic acids at the low femtomole level. *Sensor. Actuator. B Chem.* 145 (1), 588–591.
- Takakado, A., Nakasone, Y., Terazima, M., 2017. Photoinduced dimerization of a photosensory DNA-binding protein EL222 and its LOV domain. *Phys. Chem. Chem. Phys.* 19 (36), 24855–24865.
- Takakado, A., Nakasone, Y., Terazima, M., 2018. Sequential DNA binding and dimerization processes of the photosensory protein EL222. *Biochemistry* 57 (10), 1603–1610.
- Terazima, M., 2022. Revealing protein reactions using transient grating method: Photo-induced heating, volume change, and diffusion change. *J. Appl. Phys.* 131 (14).
- Vogt, A., Paulat, R., Parthier, D., Just, V., Szczepek, M., Scheerer, P., Xu, Q., Möglich, A., Schmitz, D., Rost, B.R., 2024. Simultaneous spectral illumination of microplates for high-throughput optogenetics and photobiology. *Biol. Chem.* 405 (11–12), 751–763.
- Wang, S., Poon, G.M., Wilson, W.D., 2015. Quantitative Investigation of protein–nucleic Acid Interactions by Biosensor Surface Plasmon Resonance, DNA-protein Interactions: Principles and Protocols. Springer, pp. 313–332.
- Zhu, L., Wang, Y., Wu, X., Wu, G., Zhang, G., Liu, C., Zhang, S., 2025. Protein design accelerates the development and application of optogenetic tools. *Comput. Struct. Biotechnol. J.*
- Zoltowski, B.D., Motta-Mena, L.B., Gardner, K.H., 2013. Blue light-induced dimerization of a bacterial LOV-HTH DNA-binding protein. *Biochemistry* 52 (38), 6653–6661.